HHS Public Access

Author manuscript

Biomaterials. Author manuscript; available in PMC 2020 July 01.

Published in final edited form as:

Biomaterials. 2019 July ; 208: 32–44. doi:10.1016/j.biomaterials.2019.04.001.

Injectable osteogenic microtissues containing mesenchymal stromal cells conformally fill and repair critical-size defects

Ramkumar T. Annamalai[a], **Xiaowei Hong**[a], **Nicholas G. Schott**[a], **Gopinath Tiruchinapally**[a], **Benjamin Levi**[b], and **Jan P. Stegemann**[a,*]

[a]Department of Biomedical Engineering, University of Michigan, Ann Arbor;

[b]Department of Surgery, University of Michigan, Ann Arbor

Abstract

Repair of complex fractures with bone loss requires a potent, space-filling intervention to promote regeneration of bone. We present a biomaterials-based strategy combining mesenchymal stromal cells (MSC) with a chitosan-collagen matrix to form modular microtissues designed for delivery through a needle to conformally fill cavital defects. Implantation of microtissues into a calvarial defect in the mouse showed that osteogenically pre-differentiated MSC resulted in complete bridging of the cavity, while undifferentiated MSC produced mineralized tissue only in apposition to native bone. Decreasing the implant volume reduced bone regeneration, while increasing the MSC concentration also attenuated bone formation, suggesting that the cell-matrix ratio is important in achieving a robust response. Conformal filling of the defect with microtissues in a carrier gel resulted in complete healing. Taken together, these results show that modular microtissues can be used to augment the differentiated function of MSC and provide an extracellular environment that potentiates bone repair.

Keywords

Bone regeneration; Microtissues; Mesenchymal stromal cells; Critical size defect; Non-invasive delivery; Chitosan and Collagen

Introduction:

Bone has a remarkable capacity to regenerate through carefully orchestrated, cell-mediated repair processes [1]. However, healing in large and complex fractures is often impaired, leading to incomplete or functionally inferior bone regeneration. In some wounds, loss of the native vasculature and infection of the wound bed can further impair bone regeneration, resulting in a variety of pathologies, including delayed-, mal-, and non-unions. In such cases, therapeutic intervention to stimulate and accelerate the healing response is required. Bone

*Corresponding Author: Jan P. Stegemann, Department of Biomedical Engineering, University of Michigan, 1101 Beal Ave., Ann Arbor, MI 48109, Tel: 734-764-8313, Fax: 734-647-4834, jpsteg@umich.edu.

grafting is a standard approach to this problem but needs invasive surgery to harvest and deliver the graft. Autologous grafts and flaps are limited in supply and can cause donor-site morbidity, including infection, hematoma, and pain [2]. Moreover, they are not suitable in 10–30% of cases due to difficulty in conforming the graft to the shape of the defect [3]. Allogeneic decellularized grafts and synthetic ceramic substitutes can also be used, but are biologically inferior compared to viable bone grafts due to the lack of cellular components. Although processes such as irradiation and lyophilization can reduce the risk of disease transmission from an allogeneic graft, they eliminate cellular components resulting in reduced osteoinductivity [4] and revascularization, resulting in higher bone resorption [5].

The ideal bone substitute would exhibit osteoconductive, osteoinductive, and osteogenic properties and would promote concomitant neovascularization of larger defects [4]. Materials-based approaches have been developed to promote osteoconductivity [1], and the immobilization and release of growth factors can be used as an osteoinductive cue. However, only cells can produce bone, and osteogenesis therefore requires either recruitment of endogenous cells or delivery of exogenous cells capable of forming bone. In large and ischemic defects, endogenous cell recruitment is impaired, and cell transplantation may be required. Approaches in which appropriate progenitor cells are delivered in osteoconductive and osteoinductive microenvironments have particular promise because they combine the elements needed to regenerate bone even in challenging situations. Adult mesenchymal stromal cells (MSC) have been widely studied in this application because of their demonstrated osteogenic potential, but only limited success has been achieved in translation to the clinic [6]. Therefore, guiding progenitor cell phenotype after transplantation is an intense field of research with the potential to create more robust methods to treat orthopedic bone defects.

Cell- and material-based strategies to bone regeneration have been successfully applied in the clinic [7], yet most approaches involve pre-formed scaffolds that require invasive surgery for implantation. Minimally-invasive delivery of cells and materials is preferable to minimize surgical complications and the possibility of infection [8]. In particular, delivery of moldable materials via injection has the advantage that they can conformally fill even irregularly-shaped defects. A variety of approaches have been developed to inject cells suspended in a protein or polymer solution, which can then be triggered to transform into a cell-laden hydrogel *in situ* [9]. Such hydrogels typically have relatively weak mechanical properties [10] unless they are chemically cross-linked, which can introduce cytotoxicity [8]. An alternate approach is to fabricate small tissue modules *ex vivo* by combining appropriate cells and extracellular matrix materials. This strategy has the advantage that the embedded cells can attach and remodel the matrix, and can be induced to proliferate and differentiate prior to being implanted via injection.

In this study, we combined adipose-derived MSC with a biomaterial matrix designed to mimic the native bone matrix and to provide osteoconductive cues. Native bone has a hierarchical structure composed of the protein collagen Type I, proteoglycans and glycosaminoglycans, and the calcium phosphate mineral hydroxyapatite [11]. We therefore developed a matrix that combined collagen (COL), which possesses motifs for cell adhesion that also guide cell function [12], with chitosan (CHI), a natural biopolymer that structurally

and compositionally resembles GAG [11]. Chitosan provides strength in compression and has been shown to have osteogenic properties [13, 14]. Exogenous hydroxyapatite (HA) was included to mimic the inorganic component of bone matrix and to provide further biochemical and physical cues through matrix reinforcement [15, 16]. Although COL-CHI composites have been previously used in the form of films [17], fibers [18], or freeze-dried sponges [19], there is far less previously reported work on their use in the form of hydrogels to encapsulate cells under physiological conditions. In the present study, we used COL-CHI-HA composite material to create modular, spheroidal microtissues (60–100 μm in diameter) containing embedded MSC and designed to be delivered via injection through a standard needle. We characterized the morphology and composition of the microtissues, as well as the viability and phenotype of the embedded MSC. Microtissues were then implanted into a critical size cranial defect to investigate the effects of cell concentration, microtissue preparation volume, and localization of microtissues in the defect site on the quantity and quality of regenerated bone. This study demonstrates that modular microtissues can be an effective, minimally-invasive, cell-based approach to treating large bone defects.

2. Materials and Methods:

2.1 Cells and biopolymers

Adipose mesenchymal stromal cells (MSC) were harvested by digesting inguinal fat pads from 6–8 week old transgenic C57BL/6 ROSA$^{mT/mG}$ mice (The Jackson Labs, Bar Harbor, ME) expressing cell membrane-localized tdTomato (mT) fluorescence in all cells/tissues. The digestion solution consisted of 0.1 wt% collagenase in calcium- and magnesium-free phosphate buffered saline (PBS; Invitrogen). The harvested single cell suspension was filtered through a 70 μm cell strainer (Corning), suspended in Dulbecco's Modified Eagle's Medium (DMEM, Invitrogen) supplemented with 10% qualified FBS and 1% penicillin and streptomycin (Invitrogen) and cultured in tissue culture dishes. After 2–3 days of culture, adherent MSC were detached using TrypLE Express reagent (Invitrogen) and culture-expanded until passage 6 for use in experiments.

The biopolymers used to make osteogenic microtissues were chitosan (>90% deacetylated, Protosan UP B 90/500, Novamatrix, Philadelphia, PA) and type I collagen (MP Biomedicals Inc., Santa Ana, CA). Chitosan stock solution was made through a two-step process. First 0.25 g of chitosan flakes were suspended in 25 ml of water and autoclaved at 121°C for 30 min. Then 30 μL of glacial acetic acid (17.4 M) was added to the cooled suspension under sterile conditions. The resulting solution (1.0 wt% chitosan in 0.02 N acetic acid) was stirred for seven days at 4 °C. The solution was then centrifuged at 10000 g to remove undissolved debris and was used for making microtissues. Collagen stock solution was prepared by dissolving 250 mg of lyophilized collagen in 62.5 ml of sterile-filtered 0.02 N acetic acid. The resulting solution (0.4 wt% collagen in 0.02 N acetic acid) was stirred at 100–200 rpm for 7 days at 4 °C. The fully dissolved collagen solution was stored at 4 °C until microtissue fabrication.

2.2 Microtissue fabrication and culture

Chitosan-Collagen (CHI-COL) microtissues were fabricated using a modification of a water-in-oil emulsification method described previously [20, 21]. Briefly, to prepare microtissues cells were suspended in a mixture of solubilized chitosan, collagen, β-glycerophosphate (58 wt% in water, Sigma), and glyoxal (68.9 mM in water, Sigma). All stock solutions were kept on ice prior to microtissue fabrication. For each 5 ml of the hydrogel mixture, 2.5 ml of the collagen stock (0.4 wt% in 0.02 N acetic acid), 1.25 ml of chitosan stock (1.0 wt% chitosan in 0.02 N acetic acid), 0.6 ml of β-glycerophosphate (58 wt% in water) and 60 μL of glyoxal (68.9 mM in water) was added and mixed thoroughly. For formulations containing hydroxyapatite, HA microparticles (reagent grade, Sigma, 1–2 μm sized particles) suspended in PBS by sonication were added at 1.0 wt%. Finally, 0.6 ml of cell suspension was added to the neutralized mixture and mixed thoroughly by gentle vortexing. The cell-hydrogel mix was then dispensed dropwise into a stirred polydimethylsiloxane (PDMS, Clearco Products, Willow Grove, PA) bath kept on ice. The mixture was stirred by a dual radial-blade impeller at 800 rpm for 5 minutes to disperse the hydrogel composite into a fine emulsion in the PDMS. After 5 min, the temperature of the bath was increased to 37 °C and it was stirred for an additional 30 minutes to achieve full gelation of the microtissue droplets. The gel droplet-in oil emulsion was then centrifuged at 200 g for 5 min to separate the microtissues from the PDMS phase. The PDMS supernatant was removed without disturbing the pellet, which was then washed twice with complete culture media and collected by centrifugation at 150 g for 5 min. Microtissues were equilibrated in 5 ml of complete culture media to remove unbound β-glycerophosphate, and were then cultured in vented tissue culture tubes in a standard CO_2 incubator at 37 °C for 48 hours before implantation. The morphology, sphericity, and size distribution of the microtissues were characterized using image stacks generated using a confocal microscope (Nikon Instruments, Melville NY). ImageJ software (National Institutes of Health) was used to characterize microtissue features.

Osteogenic differentiation of MSC embedded in microtissues was stimulated using standard osteogenic medium supplements: 0.2 mM ascorbic acid-2 phosphate (Sigma, St. Louis, MO), 10 mM β-glycerophosphate (Sigma), and 100 nM dexamethasone (Sigma). The phenotype of cells embedded in microtissues was characterized at day 0, 7, 14, and 21. Alkaline phosphatase (ALP) activity was quantified using a commercially available kit (Abcam, Cambridge MA) according to the manufacturer's instructions. Similarly, osteocalcin secretion was assayed using a commercially available mouse osteocalcin ELISA kit (Novus Biologics, Centennial, CO) according to the manufacturer's instructions. The orthocresolphthalein complex one (OCPC) method was used to quantify calcium deposition as previously described [21]. Briefly, a working solution consisting of 0.05 mg/mL of OCPC in ethanolamine-boric acid-8-hydroxyquinoline buffer was added to samples and standards ($CaCl_2$, Sigma) suspended in 1 N acetic acid. After 15 min of incubation at room temperature, absorbance was measured at 575 nm. Cell proliferation was quantified through total DNA measurement using a DNA assay kit (Quanti-iT™ PicoGreen dsDNA kit; Invitrogen). The total DNA values were used to normalize ALP, osteocalcin and calcium deposition.

2.3 Mouse calvarial defect and implantation

All animal procedures were performed in compliance with the Guide for the Care and Use of Laboratory Animals at the University of Michigan and approved by the Chancellor's Animal Research Committee. All live animal surgical procedures were performed under 3–5% isoflurane/oxygen anesthesia. Immediately after induction, buprenorphine (0.05–0.1 μg/g body weight) and Xylazine (1.5 mg/kg) were administered for analgesia before the first surgical incision. To prevent corneal dryness, a bland ophthalmic ointment was applied during surgery. Sterile pharmacy grade saline was also administered (0.02 mL/g body weight) subcutaneously, to prevent dehydration. The calvarial defect was surgically created as previously described [22]. Briefly, after cleaning the surgical site with Betadine, a 1.5–2 cm incision was made just off the sagittal midline in order to expose the right parietal bone. The periosteum enveloping the skull (pericranium) was removed using a sterile cotton swab. Using a diamond-coated trephine bit and copious saline irrigation, a unilateral 4 mm full-thickness critical-sized calvarial defect was created in the non-suture associated right parietal bone, taking care to avoid dural injury. After injecting the microtissue preparation into the defect, the skin was sutured with 6–0 vicryl suture, and the animals were monitored as per the established post-operative animal care protocols. Animals were kept under warm pads during recovery and observed for 6 h before being returned to the animal housing facility. Animals were monitored twice daily for three days and weekly thereafter to ensure postoperative recovery. Buprenorphine was administered every 12 hours for two days postoperatively.

In studies using osteogenically predifferentiated MSC, the fabricated microtissues were cultured in osteogenic media for 7 days before implantation. Preliminary studies showed that microtissue formulations lacking an HA component failed to produce appreciable ossification in the calvarial defect. Therefore, HA was included in all tested formulations. For implants using a fibrin carrier gel, 1.0 mL of microtissues were combined with 625 μL of fibrinogen (2.5 mg/ml) in PBS, 20 μL of thrombin (1 U/mL), and 100 μL of FBS. Fibrin gels (final concentration of 2.5 mg/ml) were immediately cast in a 24-well plate with 0.5 mL of the mixture in each well and incubated at 37 °C for 45 min to allow complete gelation. A 4 mm biopsy punch was used to make a plug of this material to fit the dimensions of the calvarial defect. The cell concentration and implant volume for the mouse calvarial defect studies are listed in Table 1.

2.4 In vivo imaging and analysis

In vivo bone formation was assessed using longitudinal micro-computed tomography (microCT), performed using a high-resolution small animal imaging system (SkyScan 1176, Bruker, Billerica, MA), for up to 15 weeks. Images were reconstructed and bone formation was analyzed using a MicroView software (GE Healthcare, London ON, Canada). Importantly, while the whole defect region was imaged, quantification of new bone formation included only the area within the calvarial defect itself, so that results could be appropriately compared across treatment groups. Quantification was performed by selecting for new, calcified bone using a threshold of Hounsfield radiodensity of 1250 or higher based on the Misch bone density classification [23]. Scanning of implants that contained only HA but had not had time to mineralize confirmed that the 1250 Hounsfield Unit threshold did

not image the HA component, but only detected new mineralization of the implants (Suppl. Fig. 1). Every mouse was scanned with a CT-phantom which included hydroxyapatite, water, and air for calibration.

To track the red fluorescent tdTomato (mT) from implanted MSC, an IVIS® Spectrum in vivo imaging system (PerkinElmer, Shelton CT) and confocal microscope (Nikon) were used. At week 12 the animals were sacrificed by CO_2 asphyxiation and cervical dislocation, and were imaged immediately after removing the skin to eliminate auto-fluorescence. The calvaria were placed in the imaging system and imaged for 2 seconds at small binning. The fluorescence at the calvarial injury site was quantified using Living Image 3.2 (PerkinElmer). The calvaria were then fixed in buffered alcoholic formalin solution (Z-Fix, Anatech) and stained for DAPI (Invitrogen). After rinsing twice in 10 mM PBS, samples were resuspended in fresh PBS and images were captured using a confocal microscope (Nikon).

2.5 NMR analysis

Nuclear magnetic resonance (NMR) spectroscopy was employed to study the composition of the microtissue matrix as previously described [24]. Briefly, collagen-chitosan microtissue samples were collected, washed in PBS, dialyzed (8 kDa MWCO) against DI water for 48 hours at 4 °C and lyophilized to obtain dry samples. Then 2.0 mg of each sample was dissolved in deuterated water (D_2O, 0.5 mL) containing 0.5% CD_3COOD and dissolved at room temperature for 4 hours before analysis. ^1H NMR spectra in D_2O were recorded on 700 MHz Varian Mercury systems (Palo Alto, CA) at room temperature. ^1H NMR spectrums were referenced using Me_4Si (0 ppm), residual D_2O at δ ^1H-NMR 4.65 ppm. ^{31}P-NMR was used to evaluate the phosphorous groups from β-GP.

2.6 Histological analysis

At 12 weeks after implantation of microtissues, animals were euthanized using CO_2 asphyxiation and cervical dislocation and tissue from the implant site was examined histologically to allow confirmation of microCT imaging results. The calvaria were harvested fixed, decalcified and paraffin-embedded as described previously [25–27]. The embedded tissues were sectioned using a microtome into 6 μm sections and stained with Pentachrome, hematoxylin and eosin dyes for analyzing neo-vessel formation, mineralization, and bone morphology. For vascularization analysis, samples were immunostained for CD31 and evaluated for microvessels as described previously [28]. The sections were then mounted and imaged with a bright-field microscope (Nikon).

2.7 Ultrasound imaging-guided in-vivo injection of microtissue

To demonstrate minimally-invasive delivery, microtissues were injected into a premade defect using a 23 gauge needle guided by ultrasound imaging. Before the procedure, the animal was euthanized using CO_2 asphyxiation to prevent pain and suffering. A 4-mm critical-sized calvarial defect was created, and the skin was immediately sutured. Hair was removed from the skin above the calvarial defect, and acoustic gel was applied to allow imaging with a high- resolution small animal ultrasound unit (Visualsonics, Toronto, Canada). Freshly-made microtissues containing 1.0 $x10^6$ MSC/mL (of initial hydrogel

solution) were concentrated by centrifugation and then injected into the defect using a 23 gauge needle. The procedure was recorded in real time using a 55 MHz center frequency transducer (Vevo 708, 6 dB bandwidth) at a rate of 11 frames/s. Three-dimensional images of the defect before and after the injection were acquired by moving the ultrasound probe with a step size of 30 μm over an 8 mm range while scanning. Spectral ultrasound analysis was performed to discriminate the native tissues and microtissue construct based on their mineral content as described previously [29, 30]. Briefly, grayscale values GS(y,z), acoustic scatterer diameter and acoustic concentration were extracted from the raw backscattered radio-frequency (RF) signals. For power spectrum analysis, each RF scan line was segmented and a linear fit was applied to the calibrated gated power spectrum to determine the slope and mid-band fit (MBF). The effective scatterer diameter was calculated from the slope, the geometry index, the center frequency of the imaging transducer, and bandwidth of the transducer.

2.8 Statistical analysis

All measurements were performed at least in triplicate. Data are plotted as means with error bars representing the standard deviation. Statistical comparisons were made using Student's *t*-test and two-way ANOVA with a 95% confidence limit. Differences with $p<0.05$ were considered statistically significant.

Results

3.1 Fabrication and characterization of chitosan-collagen osteogenic microtissues

The microtissue fabrication process and characterization of the resulting tissue modules are shown in Figure 1. The water-in-oil emulsification method (shown schematically in Fig. 1A) consistently produced spheroidal microtissues containing uniformly embedded MSC. COL-CHI microtissues had an average diameter of 54.3±12.1 μm (Fig. 1B). Addition of HA microparticles to enhance calcification increased the size of microtissues in a dose-dependent fashion, with the diameter of 0.5%, 1%, and 2% HA CHI-COL microtissues being 73.9±17.7 μm, 79.7±18.7 μm, and 148.6±21.4 μm respectively. Addition of 0.5×10^6 cells/ml yielded microtissues with an average diameter of 84.6 ±18.2 μm. Increasing the cell concentration did not significantly affect the average diameter of the cell-laden microtissues. DNA quantification indicated a cell encapsulation efficiency of 88.5% at cell concentrations between $0.5–1.5\times10^6$ cells/mL of the hydrogel. At a concentration of 1.0×10^6 cells/mL, a single 100 μm diameter microtissue contained approximately 5–10 cells. Microtissues with $0.5\ x10^6$ cells/ml and 1% HA had a diameter of 81.1±20.1 μm, and were not statistically significantly different from those containing only 0.5 or only 1.0% HA.

In vitro characterization showed that the microtissues were stable and remained as individual modules in culture while maintaining high cell viability (Fig. 1C). Cell viability remained high over at least 21 days in culture, while the proliferation rate of osteogenically differentiated MSC in microtissues was markedly lower than control, undifferentiated MSC (Suppl. Fig. 2). Exposure to osteogenic supplements in culture resulted in clear increases in makers of osteogenesis over 14 days in culture, including the secretion of increased levels of alkaline phosphatase and osteocalcin, and the deposition of calcium mineral (Fig. 1D). NMR

analysis of the matrix composition showed that collagen and chitosan have distinct spectra, and demonstrated the presence of both components in the microtissues (Fig. 1E). Further NMR analysis of the microtissues over time showed that the matrix composition was maintained over three weeks in culture (Refer to Suppl. Fig. 3 for detailed analysis).

3.2. Bone regeneration in critical-sized calvarial defects

Microtissue implants were tested for the ability to regenerate bone in a full-thickness critical size cranial defect in the mouse. In a first study, the effect of the cellular component was examined, as shown in Figure 2. Microtissues (created using 1 ml of initial hydrogel volume) with no cells, undifferentiated MSC (1.0×10^6 cells/mL of the hydrogel), or osteogenically predifferentiated MSC (OD-MSC, 1.0×10^6 cells/mL of the hydrogel) were implanted for 15 weeks with regular periodic assessment by microCT, as well as histological analysis at explant. Gross examination of the 3D reconstructed microCT images showed that by week 10, osteogenically predifferentiated microtissues had bridged >95% of the defect area ($p<0.001$, Fig. 2A). In contrast, microtissues with undifferentiated MSC showed significantly less bony bridging ($p<0.05$) with only ~50% coverage. Microtissues without cells showed the lowest degree of defect bridging, covering only ~30% of the defect area. Correspondingly, the total bone volume, bone mineral content, bone mineral density and bone volume fraction (bone volume/tissue volume) of the newly formed bone within the defect was significantly higher in the osteogenically predifferentiated microtissues compared to the acellular and undifferentiated MSC conditions ($p<0.001$, Fig. 2B–E). Histological analysis of the newly formed bone in osteogenically-predifferentiated samples revealed a lamellar and woven bone morphology, high collagen deposition (yellow staining) and structures resembling early marrow cavities (Fig. 2F). There was evidence of integration with the native bone, particularly in osteogenically predifferentiated implants. Microtissues containing undifferentiated MSC exhibited only minimal bone formation at the defect borders and generally low collagen deposition and were characterized by sparse bone spicules surrounded by fibrous connective tissue. The microtissues without cells had the lowest mineral content, though the defect was fully bridged with collagenous osteoid structures interspersed with blood vessels (Fig. 2F).

3.3. Influence of microtissue implant volume and cell concentration on bone formation

The robust and voluminous bone formation resulting from the implantation of osteogenically predifferentiated microtissues (OD-MSC) extended beyond the defect site and produced superfluous tissue adjacent to the defect. The volume of microtissues delivered was therefore varied to determine the most effective delivery bolus for regeneration of bone in the defect site. Implants were made using osteogenically predifferentiated microtissues created using 0.25 mL, 0.50 mL and 0.75 mL of initial hydrogel volume, at a constant cell concentration of 0.5×10^6 cells/mL of the hydrogel. These microtissue preparations were implanted into a critical size cranial defect in the mouse, and the results are shown in Figure 3. Characterization of bone formation at 0, 3, 6, 9 and 12 weeks post-implantation using microCT showed that the volume of new bone decreased with decreasing initial volume of the microtissue implant (Fig. 3A). There was no statistical difference in bone volume between the highest and medium amounts tested, but new bone volume dropped significantly at the lowest implant volume (Fig. 3B). A similar dose-dependence was

observed in bone mineral content (Fig. 3C), bone mineral density (Fig. 3D) and bone volume fraction (Fig. 3E), with lower implant volumes generally leading to less robust regeneration. Consistent with the radiographic analysis, histological analysis of the calvaria at 12 weeks showed less apparent formation of lamellar and woven bone as the microtissue implant volume decreased (Fig. 3F).

The influence of the cell concentration used in the microtissue implants was also investigated, which keeping the implant volume constant. Microtissue implants containing OD- MSC microtissues made at concentrations of 1.0×10^6, 2.0×10^6 and 3.0×10^6 cells/mL were studied in the mouse critical size cranial defect, as shown in Figure 4. Interestingly, an increase in cell concentration reduced the degree of ossification of microtissues and volume of bony structures in the defects (Fig. 4A) in a dose-dependent manner. Higher cell concentration resulted in significantly reduced new bone volume (Fig. 4B), bone mineral content (Fig. 4C), and total bone fraction (Fig. 4E), while the lowest cell concentration consistently outperformed the medium- and high concentration implants in these metrics. The bone mineral density, however, stayed essentially the same between the groups (Fig. 4D). Histological analysis revealed lamellar and woven bony structures with collagen deposition within the defect in all conditions, but larger areas of ossified regions were seen in implants at lower cell concentration (Fig. 4F).

3.4. Delivery of microtissues in a fibrin carrier gel

The open nature of the critical size calvarial defect makes it difficult to contain microtissues only within the defect site. Therefore the effect of concentrating the microtissue population in the defect using a fibrin carrier gel was examined, as shown in Figure 5. Microtissues made with OD-MSC were suspended in a fibrin gel, and a plug of this material was prepared to fit the dimensions of the calvarial defect. These implants were compared to similar microtissues transplanted as a paste, and microtissues created with undifferentiated MSC served as an additional control. MicroCT imaging showed clearly that the carrier gel effectively contained the microtissues within the calvarial defect and conformed closely to the defect area (Fig. 5A). Within nine weeks the defect was bridged entirely in both the OD-MSC conditions with evidence of active remodeling. Quantitative analysis of microCT data showed no significant difference in the new bone volume between the OD-MSC microtissues implanted with or without a carrier gel and both groups significantly outperformed the implants with undifferentiated MSC (Fig. 5B). Likewise, the mineral density, mineral content and bone volume fraction were markedly higher in the OD-MSC implants, though there were no significant effects of the use of a carrier gel (Fig. 5C–F). Histological analysis revealed dense collagenous lamellar and woven bone formation in OD-MSC implants, compared to much looser and less defined structures in the undifferentiated microtissue implants (Fig. 5F). Analysis of vascularization of the newly formed tissues showed that implants with OD-MSC had significantly higher blood vessel area (Fig. 5G), with well-developed blood vessels perfusing the implant volume (Fig. 5H). Fluorescent imaging of the calvaria using an in vivo imaging system showed the presence of fluorescently tagged exogenous MSC in all conditions at week 12 (Suppl. Fig. 4), confirming the engraftment of the implanted cells.

3.5. Ultrasound-guided minimally invasive delivery of microtissues

The ability to deliver microtissue implants via injection was demonstrated by administering them directly through the skin to the calvarial defect in a mouse through a standard 23G hypodermic needle (330 μm inner diameter). Microtissue delivery was guided by high-resolution spectral ultrasound imaging to track progress in real time and to provide information on the composition of the implants (Fig. 6A). Ultrasound imaging enabled the creation of 3D spatial maps of the defect and the surrounding tissues, and periodic images showed the transfer of the microtissue paste into the implant side (Fig. 6B). The spectral ultrasound imaging (SUSI) technique applied in this study was also used to quantify the mineral content of the implanted tissues. Microtissues with varying HA concentration were imaged and analyzed, showing that the acoustic concentration parameter varied linearly with mineral content (Fig. 6C). This allowed the generation of spatial maps of the mineral concentration within 3D constructs (Fig. 6D). These non-destructive ultrasound imaging and analysis techniques can be used to monitor cell delivery, and potentially also can be applied to noninvasive and quantitative longitudinal monitoring of implant ossification and defect healing.

4. Discussion

Despite progress in developing new treatments for complex fractures and large bone defects over the past decade, there remains an important need for stimulating bone regeneration in a variety of serious indications [31, 32]. There is a mismatch between the clinical demand for advanced therapies and the degree to which clinical translation has been achieved. Importantly, the desired properties of a tissue-engineered bone substitute depend on the intended clinical use. Fractures in large, load-bearing bones require mechanical stability and the regeneration of structurally strong bone. In other indications, the defect may not be load-bearing, but associated soft tissue loss and a challenging healing environment require a therapy that can potentiate the healing process. Therapies that can be delivered without major surgery are particularly attractive because they reduce the chance of infection and the burden of recovery. Injectable, cell-based approaches such as the one described here may therefore have particular value in treating large and complex bone defects.

The availability of an autologous cell source is an essential advantage for a cell therapy to avoid immune complications. The adipose-derived MSC used in this study can be easily obtained from the stromal vascular fraction of lipoaspirate [33]. These cells are highly proliferative [22, 34] and have verified potential to differentiate toward osteogenic, adipogenic, and chondrogenic lineages [35–38]. The extracellular matrix used in this study was chosen because of its structural and biochemical resemblance to the early bone matrix. It combines the protein collagen Type I with the GAG-like polysaccharide chitosan and further includes a hydroxyapatite mineral phase to nucleate bone formation. The process used to create cell-laden microtissues using these matrix materials is facile and allows tailoring of the size and composition of the microtissues to suit the intended application [39]. In particular, our studies demonstrated that microtissues made from MSC embedded in a CHI-COL-HA matrix maintain cell viability and are supportive of osteogenic differentiation in vitro. While the size of the microtissues depended to some degree on their composition, it

was straightforward to create osteogenic microtissues with a diameter of 60–100 microns, which was the target range for modules to be easily injectable through standard needles.

The goal of this therapy was to fully bridge a large, critical size defect in the mouse calvarium. Interestingly, transplantation of acellular microtissues (i.e., the CHI-COL-HA matrix alone) for 15 weeks resulted in some bony tissue formation, but only in apposition to the native bone of the skull, while the defect was filled mainly with loose, collagenous osteoid. These results suggest that the biomaterial alone is osteoconductive, but does not have strong osteoinductive properties. The incorporation of undifferentiated MSC into microtissues resulted in less collagen deposition, but created islands of calcified bone in the defect by week 15, and the total new bone volume within the defect was not significantly higher than that formed by acellular microtissues. In contrast, osteogenically predifferentiated MSC resulted in a very robust bone formation that completely bridged the defect, and in fact, extended beyond the boundaries of the defect when the implant was not constrained.

The difference in the effect of undifferentiated and predifferentiated MSC in microtissues after implantation may be a result of their distinct immunomodulatory and anti-inflammatory roles [40]. Adipose-derived MSC lack the HLA-DR receptor [41], an MHC class II receptor and antigen-presenter that is commonly implicated in graft loss. In addition, MSC are known to reduce inflammation through the secretion of prostaglandin E2 (PGE2), which can suppress lymphocyte action [42] and reprogram macrophages to an anti-inflammatory phenotype [43, 44]. However, it has been shown that pro-inflammatory signals secreted by macrophages are essential in the osteogenic function of MSC. For example, tumor necrosis factor-alpha (TNFα) and interleukin 6 (IL-6) are both critical pro-inflammatory cytokines that are secreted by activated macrophages, and both have been shown to play an essential role in the osteogenic commitment of adipose-derived MSC [45, 46]. Therefore, the anti-inflammatory effects of cytokines secreted by undifferentiated MSC may be responsible for the reduced bone regeneration observed when these cells are transplanted in microtissues. However, further analyses are necessary to confirm the immunomodulatory effects of MSC in this regeneration model.

In this study, OD-MSC were predifferentiated toward the osteogenic lineage using dexamethasone, a regulator of the osteogenic transcription factor Runx2 [47], and β-glycerophosphate, a phosphate source for mineralization. It has been shown that similarly predifferentiated MSC interact with macrophages after transplantation to improve defect healing [48]. In addition, priming of MSC toward the osteogenic lineage with potent biochemical factors such as bone morphogenetic protein-2 (BMP-2) [49], platelet-derived growth factor (PDGF) [50], and TNFα [51] prior to transplantation has been shown to be effective in regenerating bone. Taken together, these results suggest that there is a benefit to predifferentiation of MSC toward the osteogenic lineage prior to transplantation, which results in increased new bone formation.

The effects of changing the implant volume and the cell concentration in implants were also investigated. Decreasing the volume of microtissues implanted had the effect of reducing lamellar bone formation, mineral deposition, and tissue remodeling. However, when the

concentration of cells in the implant was increased, there was an apparent decrease in resulting bone formation and remodeling. Interestingly, both increasing the absolute implant volume and increasing the cell concentration per volume has the effect of transplanting a larger number of cells. However, only in the case where cells were transplanted with a correspondingly increased volume of extracellular matrix was there a positive effect on bone formation. It is possible that implants with a high cell density suffer from hypoxia [52–54], which can lead to tissue necrosis [55]. Studies have shown that hypoxia (<2% oxygen) upregulates proliferation and the expression of VEGF-A in MSC [56]. However, hypoxia also suppresses the osteogenic transcription factor Runx2 via HIF-1α [57, 58]. In our study, we saw vascularized osteoid formation when high cell concentrations were delivered, but the amount of regenerated bone was decreased under these conditions. Alternately, there may be other beneficial effects of cell-matrix contacts that lead to better osteogenic outcomes in microtissues that have a lower cell concentration. Overall, it appears that maintaining an appropriate ratio of cells to the matrix is essential in maximizing the regenerative potential of MSC.

Two modes of delivering microtissue implants were examined. A primary advantage of the modular microtissue format is that they can be transplanted minimally invasively through a standard needle. The injectability of microtissues was demonstrated under guidance and monitoring by high-resolution ultrasound imaging. Filling of the defect through the skin was facile. However, it was observed that implants of microtissue paste extended beyond the boundaries of the cranial defect and produced ectopic bone in the peri-defect region. It should be noted that this issue is at least partially an artifact of the implant model used, since the intracranial pressure and geometry of the cranial defect is not conducive to retaining implanted material. Other indications, such as segmental defects surrounded by soft tissue, spinal fusions, and more enclosed cavital defects may be more appropriately filled with microtissue paste without loss of material. To address the issue of containment of microtissues in an open defect, a study was performed to examine the use of a polymerizable, fibrin-based carrier gel to entrap and retrain the microtissues. Fibrin was chosen as a carrier material because of its relative abundance, ease of handling, and wide use as a surgical sealant [59]. Also, fibrin has been shown to be effective in promoting angiogenesis [60, 61], as well as in creating vascularized tissues including bone [62, 63]. The fibrin gel carrier was effective in retaining the microtissues within the defect, and these implants resulted in similarly robust bone morphology, collagen deposition, and mineral content as unconstrained implants. In vivo imaging demonstrated that exogenous MSC were present at the implant site for the duration of the study.

This study demonstrates that injectable, MSC-laden chitosan-collagen microtissues can be used to bridge large bone defects with vascularized lamellar and woven bone. Osteogenic priming of the microtissues showed a clear benefit in accelerating bone regeneration. Importantly, the microtissue format allows osteogenic preculture and subsequent transplantation of microtissues without disrupting cell-matrix contacts. Therefore, the phenotype of cells in microtissues is likely to be preserved post-transplantation, and cells are more likely to engraft and survive in challenging healing environments. In contrast, transplantation of undifferentiated MSC in microtissues was less effective in forming new bone compared to that of acellular microtissues, possibly through mediation of the

inflammatory response. The role of MSC phenotype and its interactions with the wound healing cascade are of great importance in developing advanced bone regeneration strategies, and there is an opportunity to capitalize on this knowledge. The chitosan-collagen biomaterial used in this study was osteoconductive, and studies that varied the transplanted cell number indicated that the ratio of cells to the matrix in the implant is essential in achieving robust regeneration. Taken together, this work shows that microtissues can be used to augment the differentiated function of MSC, and to provide a suitable extracellular environment to promote bone repair and integration, while also allowing guided and minimally-invasive delivery to defect sites.

Supplementary Material

Refer to Web version on PubMed Central for supplementary material.

Acknowledgments:

Research reported in this publication was supported in part by the National Institute of Arthritis and Musculoskeletal and Skin Diseases (R01AR062636, to JPS), the National Institute of Dental and Craniofacial Research (R01DE026630, to JPS). BL is supported by funding from NIH/National Institute of General Medical Sciences Grant K08GM109105–0, NIH/National Institute of Health R01 GM123069 and R01 AR071379, American College of Surgeons Clowes Award and the International FOP Association. The content is solely the responsibility of the authors and does not necessarily represent the official views of the National Institutes of Health.

References:

1. Henkel J, et al., Bone Regeneration Based on Tissue Engineering Conceptions - A 21st Century Perspective. Bone Res, 2013 1(3): p. 216–48. [PubMed: 26273505]
2. Dimitriou R, et al., Complications following autologous bone graft harvesting from the iliac crest and using the RIA: A systematic review. Injury, 2011 42(Supplement 2): p. S3–S15.
3. Arrington ED, et al., Complications of iliac crest bone graft harvesting. Clin Orthop Relat Res, 1996(329): p. 300–9.
4. Janicki P and Schmidmaier G, What should be the characteristics of the ideal bone graft substitute? Combining scaffolds with growth factors and/or stem cells. Injury, 2011 42(Supplement 2): p. S77–S81. [PubMed: 21724186]
5. Wang S, et al., Maintenance of phenotype and function of cryopreserved bone-derived cells. Biomaterials, 2011 32(15): p. 3739–49. [PubMed: 21367449]
6. Bianco P and Robey PG, Stem cells in tissue engineering. Nature, 2001 414(6859): p. 118–21. [PubMed: 11689957]
7. Chatterjea A, et al., Clinical Application of Human Mesenchymal Stromal Cells for Bone Tissue Engineering. Stem Cells International, 2010 2010: p. 12.
8. Chang B, et al., Injectable scaffolds: Preparation and application in dental and craniofacial regeneration. Mater Sci Eng R Rep, 2017 111: p. 1–26. [PubMed: 28649171]
9. Liu M, et al., Injectable hydrogels for cartilage and bone tissue engineering. Bone Res, 2017 5: p. 17014. [PubMed: 28584674]
10. Dreifke MB, Ebraheim NA, and Jayasuriya AC, Investigation of potential injectable polymeric biomaterials for bone regeneration. Journal of biomedical materials research. Part A, 2013 101(8): p. 2436–2447. [PubMed: 23401336]
11. Barrère F, et al., Advanced biomaterials for skeletal tissue regeneration: Instructive and smart functions. Materials Science and Engineering: R: Reports, 2008 59(1): p. 38–71.
12. Shoulders MD and Raines RT, Collagen Structure and Stability. Annual Review of Biochemistry, 2009 78(1): p. 929–958.

13. Chicatun F, et al., 8 - Collagen/chitosan composite scaffolds for bone and cartilage tissue engineering A2 - Ambrosio, Luigi, in Biomedical Composites (Second Edition). 2017, Woodhead Publishing p. 163–198.
14. Venkatesan J and Kim SK, Chitosan composites for bone tissue engineering--an overview. Mar Drugs, 2010 8(8): p. 2252–66. [PubMed: 20948907]
15. Du C, et al., Formation of calcium phosphate/collagen composites through mineralization of collagen matrix. Journal of Biomedical Materials Research, 2000 50(4): p. 518–527. [PubMed: 10756310]
16. Dubey DK and Tomar V, Role of the nanoscale interfacial arrangement in mechanical strength of tropocollagen–hydroxyapatite-based hard biomaterials. Acta Biomaterialia, 2009 5(7): p. 2704–2716. [PubMed: 19345162]
17. Wang X, et al., The mechanism of a chitosan-collagen composite film used as biomaterial support for MC3T3-E1 cell differentiation. Scientific Reports, 2016 6: p. 39322. [PubMed: 28000715]
18. Hirano S, et al., Wet spun chitosan–collagen fibers, their chemical N-modifications, and blood compatibility. Biomaterials, 2000 21(10): p. 997–1003. [PubMed: 10768751]
19. Arpornmaeklong P, Pripatnanont P, and Suwatwirote N, Properties of chitosan–collagen sponges and osteogenic differentiation of rat-bone-marrow stromal cells. International Journal of Oral and Maxillofacial Surgery, 2008 37(4): p. 357–366. [PubMed: 18272341]
20. Wang L and Stegemann JP, Glyoxal crosslinking of cell-seeded chitosan/collagen hydrogels for bone regeneration. Acta Biomater, 2011 7(6): p. 2410–7. [PubMed: 21345389]
21. Wise JK, et al., Synergistic enhancement of ectopic bone formation by supplementation of freshly isolated marrow cells with purified MSC in collagen-chitosan hydrogel microbeads. Connect Tissue Res, 2016 57(6): p. 516–525. [PubMed: 26337827]
22. Levi B, et al., Human adipose derived stromal cells heal critical size mouse calvarial defects. PLoS One, 2010 5(6): p. e11177. [PubMed: 20567510]
23. M. CE, Density of Bone: Effects on surgical approach and healing, in Contemporary Implant Dentistry, Misch CE, Editor. 2008, Elsevier: Canada p. 645–667.
24. Clayden N and Williams R, Peptide group shifts. Journal of Magnetic Resonance (1969), 1982 49(3): p. 383–396.
25. Agarwal S, et al., Inhibition of Hif1alpha prevents both trauma-induced and genetic heterotopic ossification. Proc Natl Acad Sci U S A, 2016 113(3): p. E338–47. [PubMed: 26721400]
26. Peterson JR, et al., Burn injury enhances bone formation in heterotopic ossification model. Ann Surg, 2014 259(5): p. 993–8. [PubMed: 23673767]
27. Ranganathan K, et al., Role of gender in burn-induced heterotopic ossification and mesenchymal cell osteogenic differentiation. Plast Reconstr Surg, 2015 135(6): p. 1631–41. [PubMed: 26017598]
28. Nor JE, et al., Engineering and Characterization of Functional Human Microvessels in Immunodeficient Mice. Lab Invest, 2001 81(4): p. 453–463. [PubMed: 11304564]
29. Gudur MSR, et al., Noninvasive Quantification of In Vitro Osteoblastic Differentiation in 3D Engineered Tissue Constructs Using Spectral Ultrasound Imaging. Plos One, 2014 9(1).
30. Hong X, et al., Multimode ultrasound viscoelastography for three-dimensional interrogation of microscale mechanical properties in heterogeneous biomaterials. Biomaterials, 2018 178: p. 11–22. [PubMed: 29902533]
31. Kneser U, et al., Tissue engineering of bone: the reconstructive surgeon's point of view. Journal of Cellular and Molecular Medicine, 2006 10(1): p. 7–19. [PubMed: 16563218]
32. Logeart-Avramoglou D, et al., Engineering bone: challenges and obstacles. Journal of Cellular and Molecular Medicine, 2005 9(1): p. 72–84. [PubMed: 15784166]
33. Mitchell JB, et al., Immunophenotype of Human Adipose-Derived Cells: Temporal Changes in Stromal-Associated and Stem Cell–Associated Markers. STEM CELLS, 2006 24(2): p. 376–385. [PubMed: 16322640]
34. Xu Y, et al., Adipose-derived mesenchymal cells as a potential cell source for skeletal regeneration. Current Opinion in Molecular Therapeutics, 2005 7(4): p. 300–305. [PubMed: 16121695]

35. Huang JI, et al., Chondrogenic potential of multipotential cells from human adipose tissue. Plast Reconstr Surg, 2004 113(2): p. 585–94. [PubMed: 14758221]
36. Gimble JM, Katz AJ, and Bunnell BA, Adipose-Derived Stem Cells for Regenerative Medicine. Circulation Research, 2007 100(9): p. 1249–1260. [PubMed: 17495232]
37. Gimble JM, et al., Adipose-derived stromal/stem cells: A primer. Organogenesis, 2013 9(1): p. 3–10. [PubMed: 23538753]
38. Mizuno H, et al., Myogenic differentiation by human processed lipoaspirate cells. Plastic and Reconstructive Surgery, 2002 109(1): p. 199–209. [PubMed: 11786812]
39. Anna B, et al., Encapsulation of adult human mesenchymal stem cells within collagen-agarose microenvironments. Biotechnology and Bioengineering, 2005 92(4): p. 492–500. [PubMed: 16080186]
40. Gao F, et al., Mesenchymal stem cells and immunomodulation: current status and future prospects. Cell Death & Disease, 2016 7(1): p. e2062. [PubMed: 26794657]
41. Gronthos S, et al., Surface protein characterization of human adipose tissue-derived stromal cells. Journal of Cellular Physiology, 2001 189(1): p. 54–63. [PubMed: 11573204]
42. Cui L, et al., Expanded adipose-derived stem cells suppress mixed lymphocyte reaction by secretion of prostaglandin E2. Tissue Engineering, 2007 13(6): p. 1185–1195. [PubMed: 17518704]
43. Qiu G, et al., Adipose-derived mesenchymal stem cells modulate CD14(++)CD16(+) expression on monocytes from sepsis patients in vitro via prostaglandin E2. Stem Cell Research & Therapy, 2017 8: p. 97. [PubMed: 28446249]
44. Németh K, et al., Bone marrow stromal cells attenuate sepsis via prostaglandin E2–dependent reprogramming of host macrophages to increase their interleukin-10 production. Nature Medicine, 2008 15: p. 42.
45. Cho HH, et al., NF-κB activation stimulates osteogenic differentiation of mesenchymal stem cells derived from human adipose tissue by increasing TAZ expression. Journal of Cellular Physiology, 2010 223(1): p. 168–177. [PubMed: 20049872]
46. Guihard P, et al., Induction of Osteogenesis in Mesenchymal Stem Cells by Activated Monocytes/Macrophages Depends on Oncostatin M Signaling. STEM CELLS, 2012 30(4): p. 762–772. [PubMed: 22267310]
47. Langenbach F and Handschel J, Effects of dexamethasone, ascorbic acid and beta-glycerophosphate on the osteogenic differentiation of stem cells in vitro. Stem Cell Res Ther, 2013 4(5): p. 117. [PubMed: 24073831]
48. Zhou Y, et al., Mesenchymal stromal cells regulate the cell mobility and the immune response during osteogenesis through secretion of vascular endothelial growth factor A. Journal of Tissue Engineering and Regenerative Medicine, 2017: p. n/a–n/a.
49. Sándor GK, et al., Adipose Stem Cell Tissue–Engineered Construct Used to Treat Large Anterior Mandibular Defect: A Case Report and Review of the Clinical Application of Good Manufacturing Practice–Level Adipose Stem Cells for Bone Regeneration. Journal of Oral and Maxillofacial Surgery, 2013 71(5): p. 938–950. [PubMed: 23375899]
50. Behnia H, et al., Repair of alveolar cleft defect with mesenchymal stem cells and platelet derived growth factors: A preliminary report. Journal of Cranio-Maxillofacial Surgery, 2012 40(1): p. 2–7. [PubMed: 21420310]
51. Lu Z, et al., Priming Adipose Stem Cells with Tumor Necrosis Factor-Alpha Preconditioning Potentiates Their Exosome Efficacy for Bone Regeneration. Tissue Engineering Part A, 2017 23(21–22): p. 1212–1220. [PubMed: 28346798]
52. Yu SP, Wei Z, and Wei L, Preconditioning strategy in stem cell transplantation therapy. Transl Stroke Res, 2013 4(1): p. 76–88. [PubMed: 23914259]
53. Valorani MG, et al., Pre-culturing human adipose tissue mesenchymal stem cells under hypoxia increases their adipogenic and osteogenic differentiation potentials. Cell Proliferation, 2012 45(3): p. 225–238. [PubMed: 22507457]
54. Han Y-S, et al., Hypoxia-induced expression of cellular prion protein improves the therapeutic potential of mesenchymal stem cells. Cell Death &Amp; Disease, 2016 7: p. e2395.

55. Greijer AE and van der Wall E, The role of hypoxia inducible factor 1 (HIF-1) in hypoxia induced apoptosis. Journal of Clinical Pathology, 2004 57(10): p. 1009–1014. [PubMed: 15452150]

56. Kakudo N, et al., Hypoxia Enhances Proliferation of Human Adipose-Derived Stem Cells via HIF-1α Activation. PloS one, 2015 10(10): p. e0139890–e0139890. [PubMed: 26465938]

57. Fehrer C, et al., Reduced oxygen tension attenuates differentiation capacity of human mesenchymal stem cells and prolongs their lifespan. Aging Cell, 2007 6(6): p. 745–757. [PubMed: 17925003]

58. Xu N, et al., Hypoxia inhibits the differentiation of mesenchymal stem cells into osteoblasts by activation of Notch signaling. Experimental and molecular pathology, 2013 94(1): p. 33–39. [PubMed: 22964414]

59. Jackson MR, Fibrin sealants in surgical practice: An overview. Am J Surg, 2001 182(2 Suppl): p. 1S–7S.

60. Annamalai RT, et al., Vascular Network Formation by Human Microvascular Endothelial Cells in Modular Fibrin Microtissues. ACS Biomaterials Science & Engineering, 2016 2(11): p. 1914–1925. [PubMed: 29503863]

61. Rioja AY, et al., Endothelial sprouting and network formation in collagen- and fibrin-based modular microbeads. Acta Biomaterialia, 2016 29: p. 33–41. [PubMed: 26481042]

62. Murphy KC, Fang SY, and Leach JK, Human mesenchymal stem cell spheroids in fibrin hydrogels exhibit improved cell survival and potential for bone healing. Cell and Tissue Research, 2014 357(1): p. 91–99. [PubMed: 24781147]

63. Rao RR, et al., Dual-phase osteogenic and vasculogenic engineered tissue for bone formation. Tissue Eng Part A, 2015 21(3–4): p. 530–40. [PubMed: 25228401]

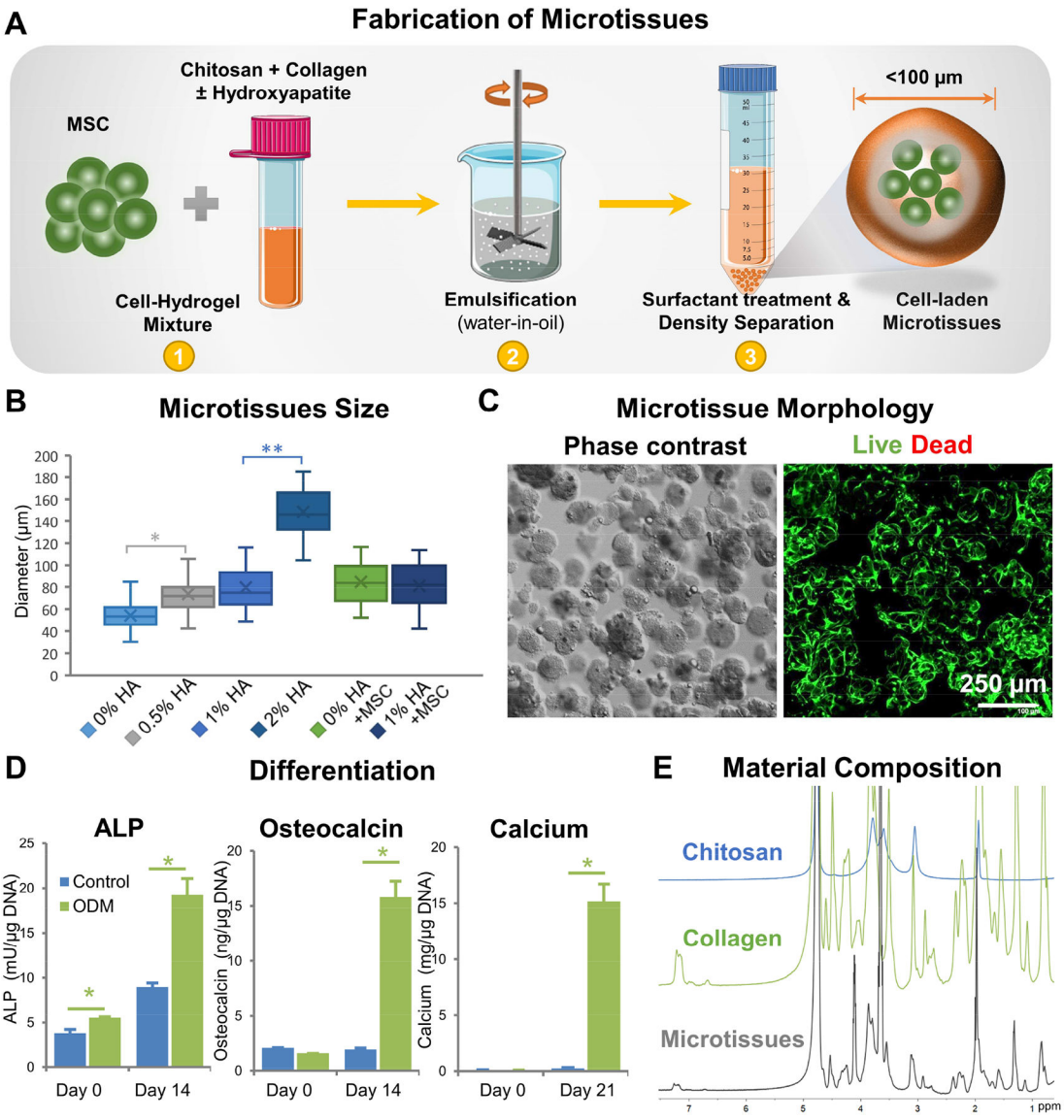

Figure 1 - Fabrication and characterization of chitosan-collagen microtissues.

A) Schematic of the water-in-oil emulsification process used to embed MSC within CHI-COL composite microtissues. B) Size distribution of CHI-COL microtissues as a function of HA content and cell loading. C) Phase contrast (Day 0) and fluorescence images (Day 14) showing the morphology of microtissues and vital staining (green) of embedded MSC, respectively. D) Expression of osteogenic markers by microtissues cultured in control and osteogenic medium (ODM) in vitro. E) ^{1}H-NMR spectra of the microtissue matrix materials, demonstrating the presence of collagen and chitosan.

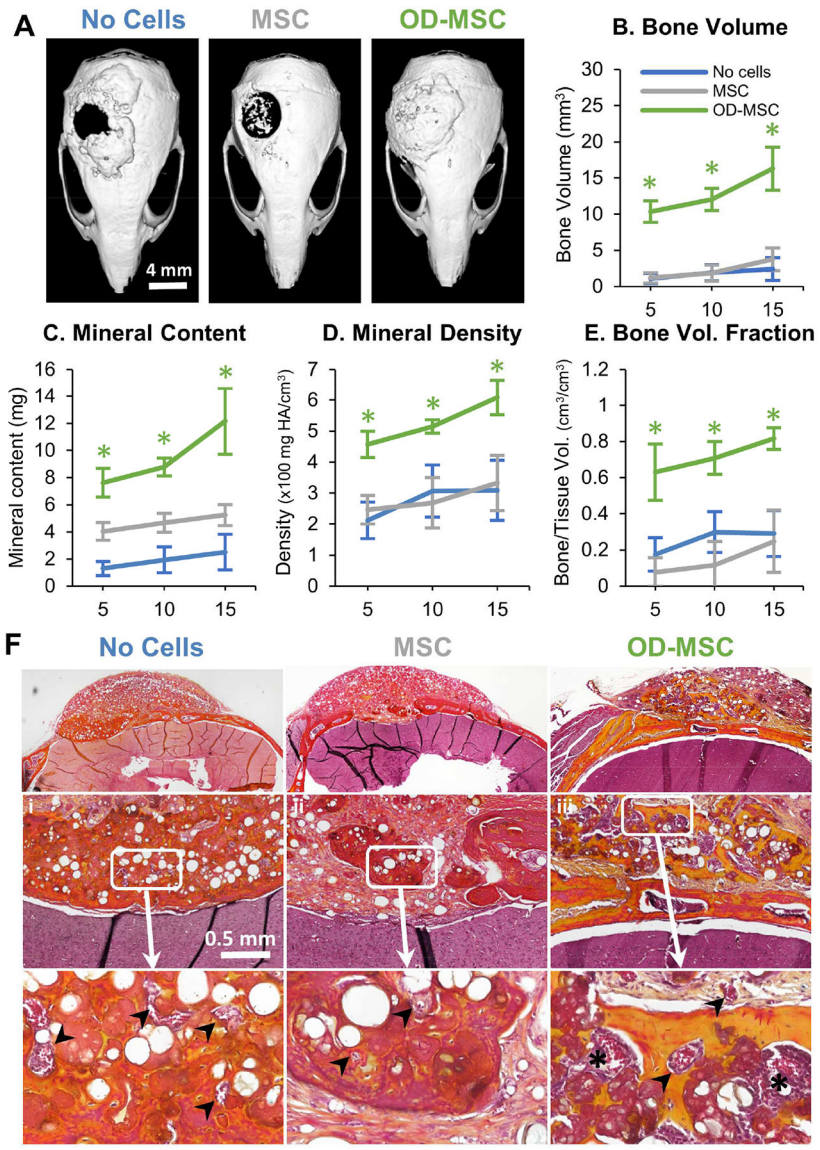

Figure 2 - Bone regeneration in a critical-sized calvarial defect.

A) Representative microCT images of bone formation in the defect region at 10 weeks. MicroCT data were analyzed to specifically assess new bone in the 4 mm defect site across implant replicates, and to obtain quantitative measures of: B) total bone volume, C) mineral content, D) mineral density, and E) bone volume fraction (bone volume/tissue volume). F) Histology images of newly formed bone in the defect site using Movat's pentachrome staining. (Collagen fibers= yellow; fibrin = bright red; nuclei = purple-black). Arrows indicate microvessels and * indicates primitive marrow cavities.

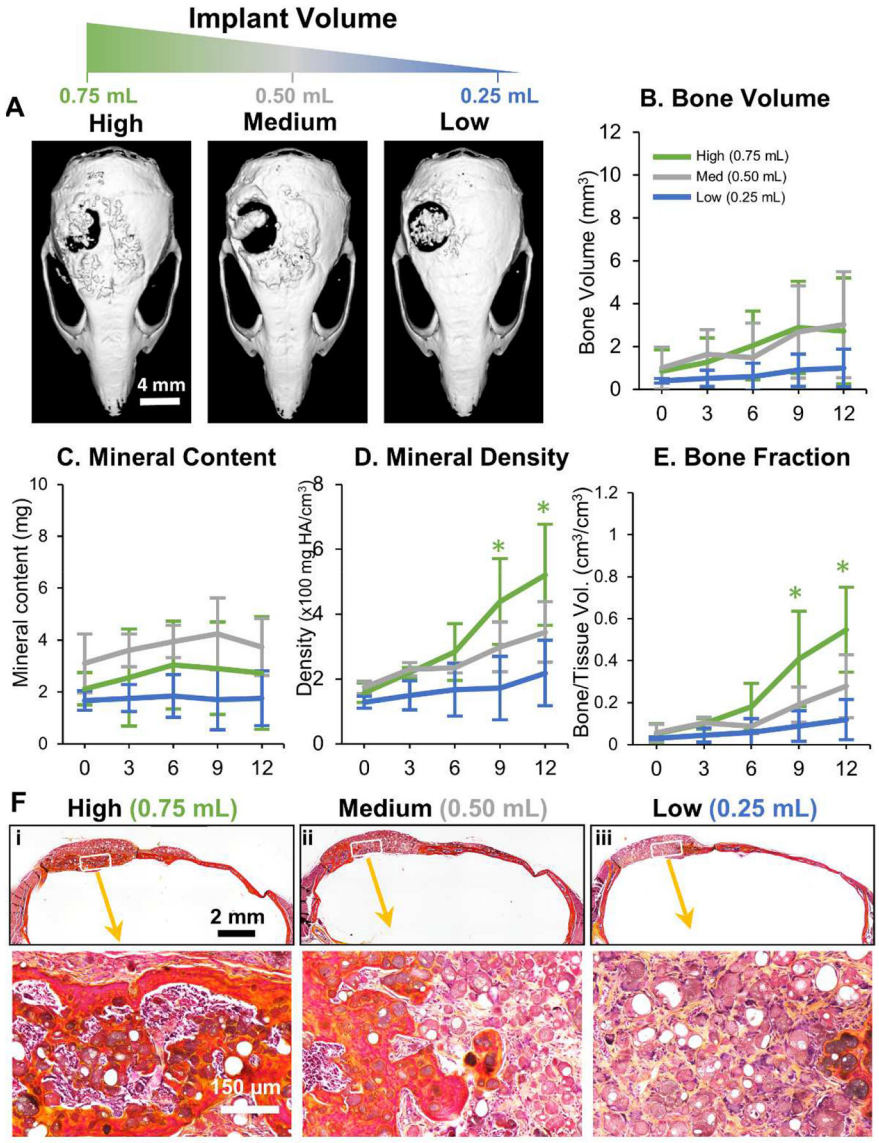

Figure 3 - Influence of microtissue implant volume on bone formation.

A) Representative microCT images of bone formation in the defect region at 12 weeks. MicroCT data were analyzed to specifically assess new bone within the 4 mm defect site across implant replicates, and to obtain quantitative measures of: B) total bone volume, C) mineral content, D) mineral density, and E) bone volume fraction (bone volume/tissue volume). F) Histology images of newly formed bone in the defect site using Movat's pentachrome staining. (Collagen fibers = yellow; fibrin = bright red; nuclei = purple-black).

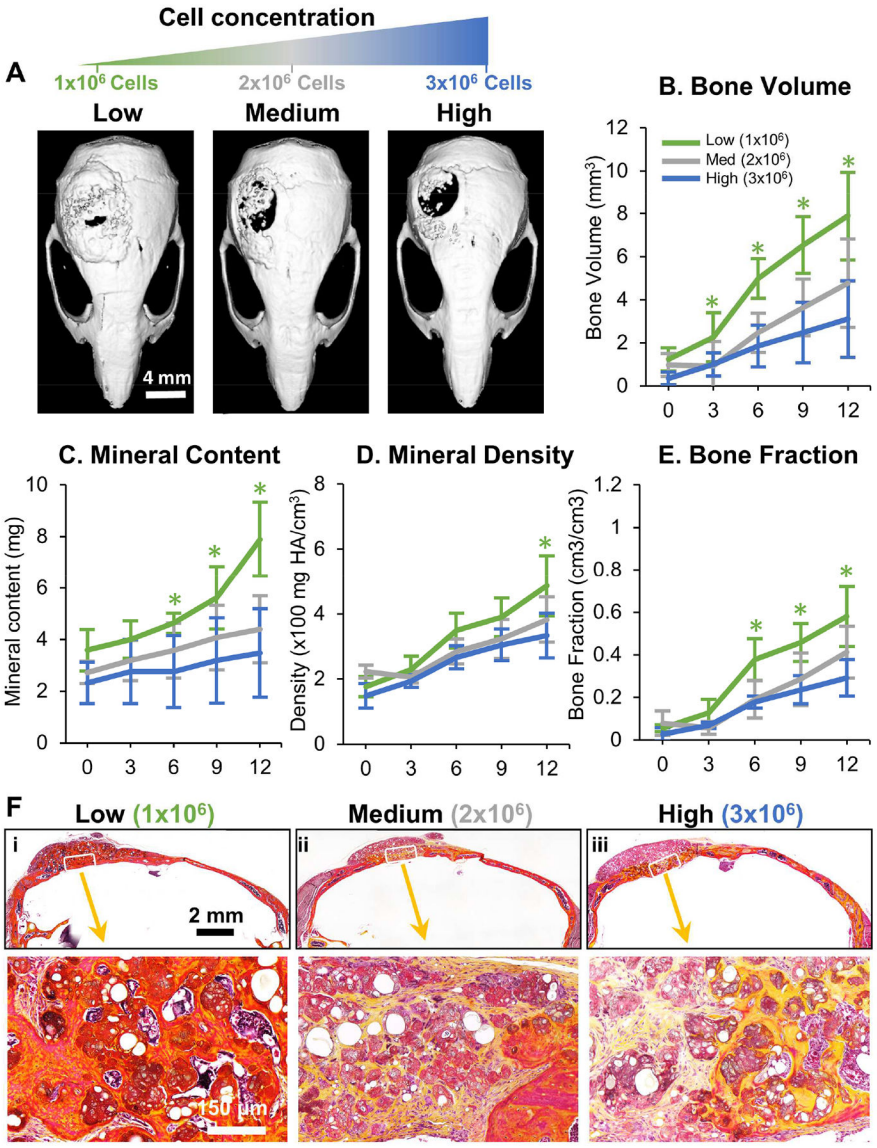

Figure 4 - Influence of cell concentration on bone formation.

A) Representative microCT images of bone formation in the defect region at 12 weeks. MicroCT data were analyzed to specifically assess new bone within the 4 mm defect site across implant replicates, and to obtain quantitative measures of B) total bone volume, C) mineral content, D) mineral density, and E) bone volume fraction (bone volume/tissue volume). F) Histology images of newly formed bone in the defect site using Movat's pentachrome staining. (Collagen fibers = yellow; fibrin = bright red; nuclei = purple-black).

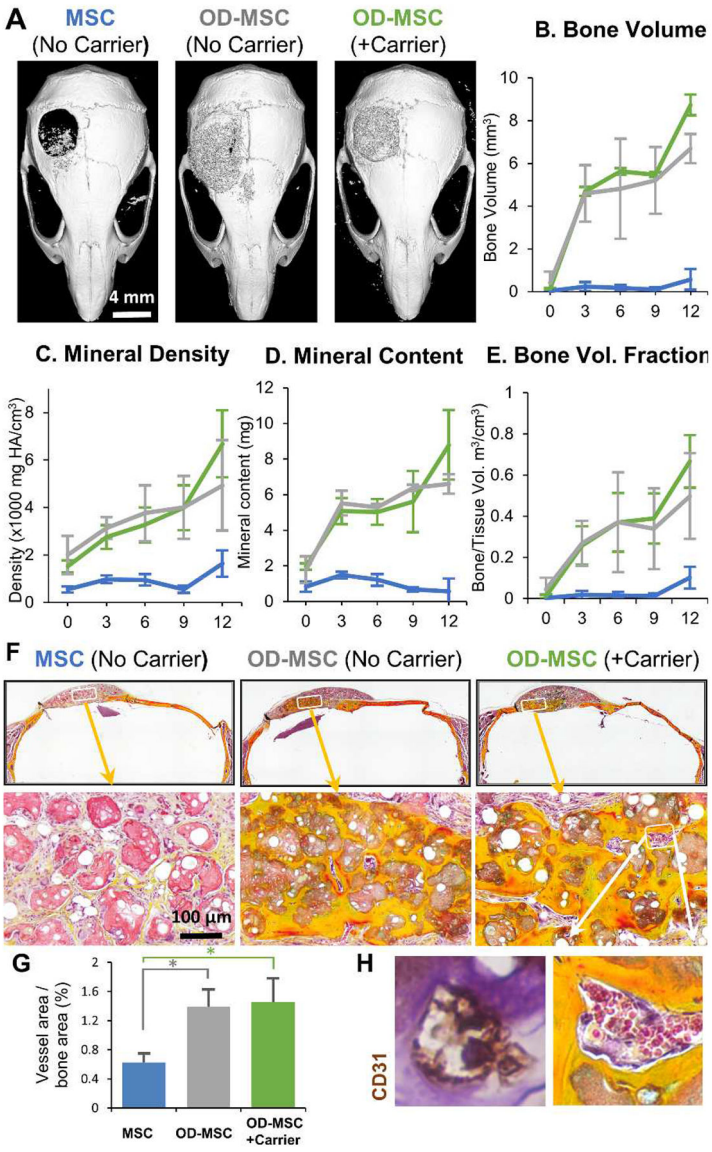

Figure 5 - Effect of microtissue delivery within a fibrin carrier gel.

A) Representative microCT images of bone formation in the defect region at 12 weeks. MicroCT data were analyzed to specifically assess new bone within the 4 mm defect site across implant replicates, and to obtain quantitative measures of B) total bone volume, C) mineral content, D) mineral density, and E) bone volume fraction (bone volume/tissue volume). F) Histology images of newly formed bone in the defect site using Movat's pentachrome staining. (Collagen fibers = yellow; fibrin = bright red; nuclei = purple-black). G) Blood vessel area within the defect was quantified from H) histology images, which showed well-developed vessels containing erythrocytes throughout the volume of OD-MSC microtissue implants.

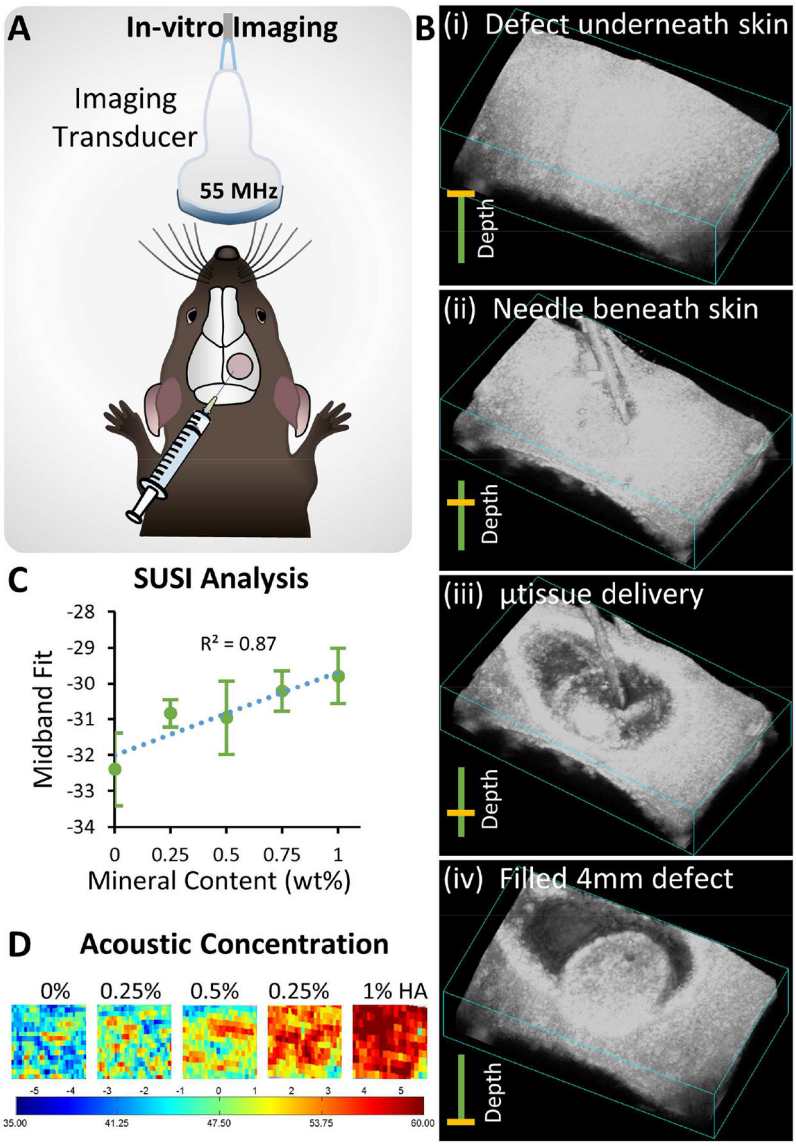

Figure 6 - Ultrasound-guided, minimally invasive delivery of microtissues.

A) Schematic of the monitoring microtissue implantation into the calvarial defect using high-resolution ultrasound imaging. B) 3D ultrasound image reconstructions showing the injection of microtissues through the skin into the calvarial defect (series i-iv). C) Correlation of mineral content of microtissues and the midband fit parameter generated by spectral ultrasound imaging (SUSI). D) Heat maps of acoustic concentration generated by SUSI, showing spatial distribution and concentration of mineral in the microtissue implants.

Table 1.

Cell density and implant volume for mouse calvarial defect studies

Experiment		Cell Concentration	Implant volume
Fig. 2	Influence of MSC differentiation state	1.0×10^6 cells/mL	1.0 mL of suspension per defect
Fig. 3	Influence of implant volume	0.5×10^6 cells/mL	0.25, 0.5, and 1.0 mL of suspension per defect
Fig. 4	Influence of MSC cell concentration	1.0, 2.0 and 3.0×10^6 cells/mL	0.5 mL of suspension per defect
Fig. 5	Influence of fibrin carrier gel	1.0×10^6 cells/mL	0.160 mL of suspension per defect